Neuron, Vol. 16, 783–795, April, 1996, Copyright ©1996 by Cell Press

Ca^{2+} Imaging of CNS Axons in Culture Indicates Reliable Coupling between Single Action Potentials and Distal Functional Release Sites

Paul J. Mackenzie, Masashi Umemiya,* and Timothy H. Murphy
Kinsmen Laboratory
Department of Psychiatry
University of British Columbia
Vancouver, British Columbia V6T 1Z3
Canada

Summary

A combination of Ca^{2+} imaging and current-clamp recording in cultured cortical neurons was used to evaluate the reliability of coupling between the action potential and rises in Ca^{2+} at distal release sites as a possible source of variability in CNS synaptic transmission. Local domains of enhanced Ca^{2+} influx were observed at varicosities on axon collaterals. Functional assay of vesicle turnover using FM1-43 and parallel electron microscopy confirmed that these varicosities were release sites. Single action potentials reliably (>95% of the time) resulted in a presynaptic Ca^{2+} transient at all presumed release sites including those on distal collaterals. Variability in the amplitude of presynaptic Ca^{2+} transients at individual boutons was estimated to be on average less than 20%. We conclude that the coupling of somatic action potentials to distal release sites is generally a reliable process, although nonlinearity in the relationship between Ca^{2+} influx and neurotransmitter release may amplify the effects of relatively small fluctuations in Ca^{2+} influx.

Introduction

The axon of a pyramidal neuron of the hippocampus or cortex is a single, highly branched process (Ramón y Cajal, 1911). Along this process, there are thousands of regularly spaced aggregates of specialized proteins that make up the sites of neurotransmitter exocytosis termed *en passant* synapses (Peters et al., 1976). Although the recent direct application of patch-clamp recording techniques to the dendrites of CNS neurons has suggested new computational roles for dendrites (Stuart and Sakmann, 1994; Spruston et al., 1995; Magee and Johnston, 1995), the behavior of individual release sites on a single mammalian axon has eluded direct physiological analysis due to their electrotonic isolation and small caliber. Previous studies of presynaptic Ca^{2+} dynamics in mammalian neurons have been limited to measurements of the averaged Ca^{2+} response over a relatively large area. These studies have defined the pharmacology of presynaptic Ca^{2+} influx (Wu and Saggau, 1994a, 1994b) and changes in transient amplitude and residual Ca^{2+} in phenomena such as long-term potentiation and facilitation (Regehr et al., 1994; Wu and Saggau, 1994c, Mintz et al., 1995). By using high resolution Ca^{2+} imaging of cultured cortical neurons, we have examined single neurotransmitter release sites to determine whether the properties of action potential-evoked Ca^{2+} influx contribute to the stochastic or unreliable nature of CNS synaptic transmission (Raastad et al., 1992; Rosenmund et al., 1993; Hessler et al., 1993; Stevens and Wang, 1994). There are several potential sources of this unreliability in synaptic transmission, including the following: variability in the threshold for action potential generation; failure of action potential conduction at axonal branch points or within a branch; variability in Ca^{2+} influx in response to action potentials that do arrive at a terminal; unreliability in the coupling of Ca^{2+} influx to vesicular release; heterogeneity in the postsynaptic response to neurotransmitter release (Wall, 1995; Allen and Stevens, 1994; Malinow, 1994; Stevens and Wang, 1995; Liao et al., 1995). To address the first three potential sources of synaptic variability, we combined high resolution Ca^{2+} imaging with current-clamp recording from presynaptic neurons. This approach has allowed us to confirm that action potentials are generated and presumably conducted along initial segments of the axon; we can therefore rule out one potential source of variability, allowing us to measure the variability due to other sources. Our results indicate that action potentials are faithfully conducted to presynaptic terminals and consistently result in Ca^{2+} influx at release sites despite the presence of axonal branches. Variability in the magnitude of the presynaptic Ca^{2+} transient between repeated trials of action potentials was low (less than 20%), but significantly different from that due to noise.

Results

Spatially Resolved Ca^{2+} Transients in Axons in Response to Action Potentials

For the majority of imaging experiments, neurons were loaded with 750 μM fura-2 K^+ salt (Grynkiewicz et al., 1985), or in some cases fluo-3 (Minta et al., 1989), using the whole-cell recording method (Hamill et al., 1981). Although this high concentration of Ca^{2+} probe would be expected to buffer peak Ca^{2+} transients and to prolong their decay, this dye concentration was required to resolve axonal processes over background fluorescence. Relatively high affinity Ca^{2+} probes (such fura-2 or fluo-3) were used to image the response to single action potentials in presynaptic terminals, in order to maximize changes in fluorescence signals in relation to baseline noise.

To resolve the presynaptic Ca^{2+} response to single or patterned action potentials, we needed to identify axons unequivocally by tracing the process from the soma to distal collaterals. We were able to accomplish this using two microscopic systems. The first, using a 100× oil immersion objective, allowed us to obtain high resolution images in previously microinjected cells; in these experiments, axonal responses were evoked using local extracellular stimulation. In other experiments, as indicated, we used a movable upright microscope with a

*Present address: Department of Neurophysiology, Tohoku University School of Medicine, Sendai 980-77, Japan.

63× water immersion objective, which allowed us to trace the axon and to evoke and measure action potentials in current-clamp mode. Axons were identified according to several criteria that are illustrated in Figure 1A (composite image). An axon was identified as a unique process that originated from the soma or from a proximal dendrite. Unlike the dendrites of most neurons we examined, the axon lacked spines (although small branches were apparent) and could be traced well beyond the dendritic field of the neuron (Figure 1Aa). In addition, we observed collateral branches that were perpendicular and appeared to maintain a constant diameter over their length, characteristic of CNS axons. The axons and their collaterals also showed varicosities at regular intervals indicative of release sites, as shown in Figure 1Ab. Only one process fitting the above description was found in each of the 119 neurons examined.

By using digital imaging with high temporal and spatial resolution, we were able to evaluate the spatial properties of Ca^{2+} transients in response to single or patterned action potentials in identified axons. Figure 1Ac shows averaged traces of Ca^{2+} response at four sites to four different stimulation patterns. We consistently observed the largest responses to single action potentials at varicosities on the smaller collateral branches of the axon, such as sites 2 and 3 (compare to sites 1 and 4 on the main branch of the axon). Although sites such as 1 and 4 showed very little response to single action potentials, we were able to evoke a consistent response by increasing the number of action potentials. A particularly dramatic example of spatial heterogeneity in these Ca^{2+} responses is shown in Figure 1B, in which a single axonal varicosity consistently shows a Ca^{2+} response severalfold greater than other dendritic or axonal sites (response to 1, 4, and 8 action potentials, averaged, accounting for the slow upstroke). Interestingly, responsive varicosities (in Figures 1A and 1B) were observed at locations that were more distal to areas that showed smaller or no response; therefore, these differences were not due to a failure of action potential conduction at the less responsive sites due to electrotonic filtering. "Hot spots" of Ca^{2+} entry at presumed neurotransmitter release sites and heterogeneity in responsiveness between sites were detected using either fura-2 (data above and Figure 5) or fluo-3 (data not shown; n = 3 cells). Axonal Ca^{2+} transients were attributed to the generation of action potentials as trials with threshold stimulation only produced Ca^{2+} transients when action potentials also occurred.

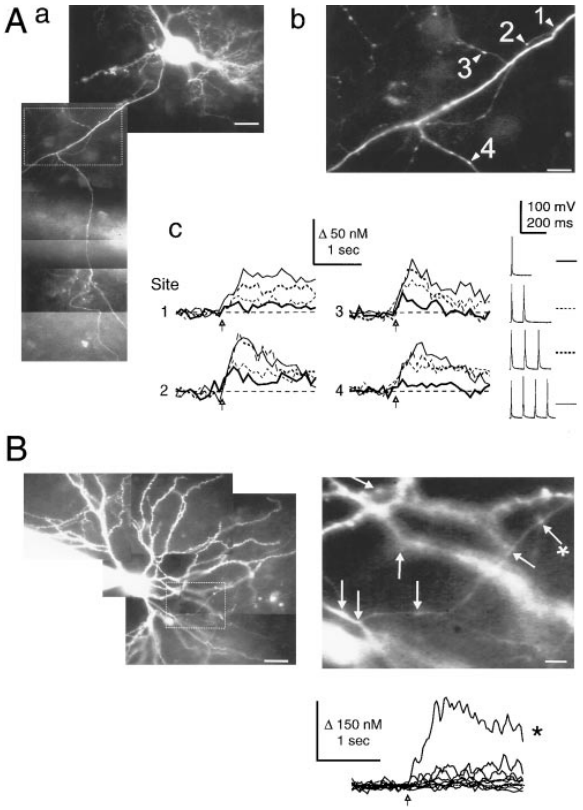

Figure 1. Spatially Resolved Ca^{2+} Transients in Axons in Response to Action Potentials

(A) (a) Composite image of a fura-2-filled cultured cortical neuron: image obtained after an experiment involving simultaneous current-clamp and Ca^{2+} imaging. Axon is shown leaving the soma and extending for at least 500 μm. Dashed line indicates area imaged during the experiment. Scale bar 25 μm. (b) Averaged fura-2 image of the main branch of the axon (~100–225 μm from soma) showing a branch point of the main axon and two thinner collateral branches. Numbered arrows indicate four sites where Ca^{2+} changes were quantified (2.4 × 2.4 μm sites). Scale bar 10 μm. (c) Quantification of Ca^{2+} responses to action potentials. (Left) Records of the response to 1, 2, 3, or 4 action potentials, at four axonal sites averaged over three trials, expressed as a change in $[Ca^{2+}]_i$. Current steps were initiated at the time indicated by arrows. Images of fura-2 fluorescence were collected at 30 Hz and averages of three buffers were calculated, background subtracted, and bleach corrected offline as described in the methods. (Right) Current-clamp records illustrating stimulation protocols (1, 2, 3, or 4 depolarizing 5 ms current steps, 10 Hz): horizontal lines to the right indicate the line style for each stimulation protocol in the plotted records (left).

(B) Highly localized Ca^{2+} response at an axonal varicosity. (Top left) Composite fura-2 fluorescence averaged image obtained with fura-2-filled pipette visible. Boxed area (broken line) indicates area imaged during the experiment. Scale bar 25 μm. (Top right) Averaged fura-2 image of the cell at rest indicating sites that were quantified (2.4 × 2.4 μm) in the Ca^{2+} traces below (indicated by arrows; one dendritic site is not shown). High responding site indicated by asterisk. Scale bar 5 μm. (Bottom) Records of change in $[Ca^{2+}]_i$ versus time for eight different sites (five axonal and three dendritic): each trace represents one site; one dendritic site is not shown. One axonal site, identified by asterisk, demonstrates a greater Ca^{2+} response to action potential stimulation. Traces were averaged responses of six trials of different stimulation protocols (1, 4, and 8 action potentials, 10 Hz). Ca^{2+} data were collected at 30 Hz, background subtracted, bleach corrected and filtered with a boxcar average of three points for presentation.

Functional Sites of Vesicular Release Show Local Ca^{2+} Transients

To determine whether the presynaptic Ca^{2+} transient is confined to an axonal varicosity, we examined averaged images of responses with high spatial resolution using a 100× (1.3 NA) oil immersion objective. The averaged image in Figure 2A indicated that Ca^{2+} transients were largely restricted to the varicosity and were considerably smaller on the flanking process that connected *en passant* synapses. Electron microscopic analysis of parallel

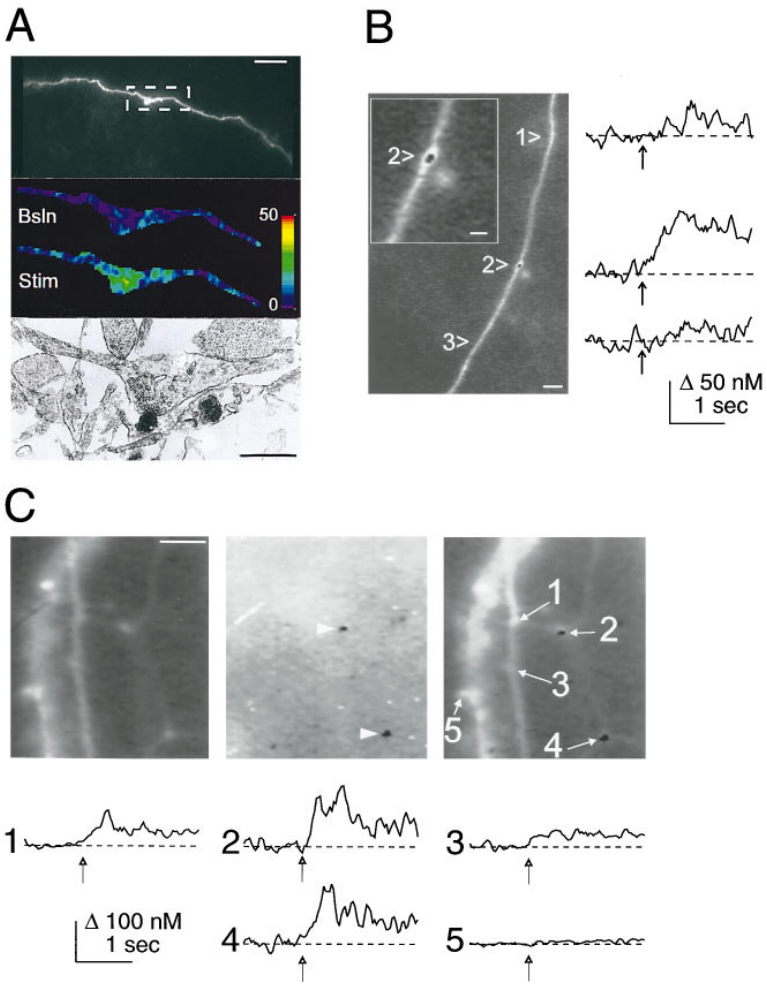

Figure 2. Functional Sites of Vesicular Release Show Local Ca^{2+} Transients

(A) High spatial resolution imaging of Ca^{2+} transients at a single varicosity obtained using a 100× objective. (Top) Averaged image of a fura-2-filled axon showing one varicosity. Scale bar 10 μm. (Middle) Enlarged images of the varicosity showing the change in $[Ca^{2+}]_i$ in response to extracellular stimulation; paired pulse, 105 ms interval; average of five stimulation trials. (Bsln) mean change in $[Ca^{2+}]_i$ immediately before stimulation, averaged over 500 ms (compared to a separate baseline period). (Stim) mean change in $[Ca^{2+}]_i$ for a 500 ms period immediately following stimulation. The color scale corresponds to a change in $[Ca^{2+}]_i$ from 0–50 nM. A boxcar filter of 2 × 2 pixels was applied to each image. (Bottom) Electron micrograph of an axonal process from a different set of cultures showing that varicosities of similar morphology contain synaptic vesicles. The dark structures correspond to dendritic spines from a biocytin-filled neuron. Scale bar 0.5 μm.

(B) An example of colocalization of FM1-43 loading and local Ca^{2+} transients at axonal varicosities (obtained using a 63× objective). (Left) Superposition of an averaged fura-2 fluorescence image with a (negative) image of FM1-43 loading: FM1-43 loading appears as a dark (black) spot that colocalizes with the varicosity at site 2 (inset). Scale bars: 5 μm; inset, 2 μm. (Right) Change in $[Ca^{2+}]_i$ versus time, in response to 8 action potentials delivered 100 ms apart in current clamp (beginning at time indicated by arrows). Records are shown for three axonal sites quantified as in Figure 1B. The largest Ca^{2+} transient was seen at site 2, the site of FM1-43 loading.

(C) An example showing colocalization of FM1-43 loading and vesicular Ca^{2+} transients from another cell (obtained using a 63× objective). (Top left) Averaged fluorescence image. Scale bar 5 μm. (Top middle) Negative image of FM1-43 loading; the darkest sites (those showing the greatest loading) are indicated by arrowheads. (Top right) Superposition of the two panels showing colocalization of varicosities and FM1-43 loading. (Bottom) Traces of change in $[Ca^{2+}]_i$ versus time in response to paired action potentials (current clamp) at four axonal sites and one dendritic site (site 5). The largest Ca^{2+} transients were observed at the varicosities (sites 2 and 4) showing FM1-43 loading.

cultures indicated that similar varicosities contained ~50 nm synaptic vesicles, as shown in Figure 2A. To determine whether the local Ca^{2+} domains that we observed were occurring at functional release sites, we used FM1-43, a marker of vesicular turnover, in combination with Ca^{2+} imaging of the same sites. Figure 2B demonstrates the close correspondence observed between localized Ca^{2+} transients and vesicular dynamics. Although all three sites demonstrated a consistent Ca^{2+} response to action potentials, the Ca^{2+} transient was consistently larger at site 2 (8 action potentials, 10 Hz, accounting for the slow upstroke). This site selectively showed loading of FM1-43 during two 15 s trains of 20 Hz action potential stimulation, suggesting that it is a functional vesicular release site (FM1-43 loading shown in black). To reduce background associated with the loading of other cells, the stimulation was confined to the fura-2 labeled neuron by using intracellular current injection. Examination of neighboring regions indicated only low levels of FM1-43 uptake in unstimulated cells, suggesting selectivity. A second example of selective FM1-43 loading is shown in Figure 2C. The left panel shows a raw fluorescence image of a dendrite, an axon, and a collateral axonal branch containing two varicosities. The middle panel shows a (negative) image of FM1-43 loading: the greatest loading occurred at the dark spots indicated by the arrowheads. The right panel is a superposition of the two panels; again, the sites of greatest vesicular turnover coincided with the collateral varicosities that consistently demonstrated the largest Ca^{2+} transients (sites 2 and 4). Selective loading of axonal varicosities with FM1-43 was observed in four neurons. Although we observed loading of these sites in response to trains of action potentials, we did not assay for unloading in these examples, since the collecting of Ca^{2+} data resulted in loss of FM1-43 fluorescence and presumed unloading of the release sites. In two neurons, selective unloading of the FM1-43 staining at axonal varicosities was observed during a 15 s train of 20 Hz. stimulation with 50% unloading occurring within 5 s (data not shown).

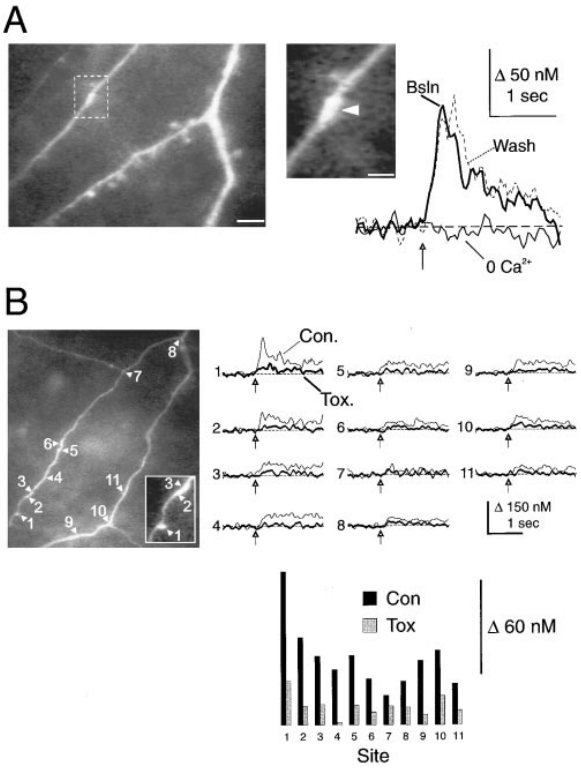

Figure 3. Dependence of Axonal Ca^{2+} Transients on Extracellular Ca^{2+} and on High Voltage–Activated Ca^{2+} Channels

(A) (Left) Averaged fura-2 image (100×) showing a dendrite and an axon with varicosity (enlarged in middle panel, arrowhead). Scale bars: 5 μm, left; 2 μm, middle. (Right) Change in $[Ca^{2+}]_i$ at the varicosity (measured over a 1.4 × 1.4 μm area) during normal extracellular Ca^{2+} (2.5 mM, Bsln), during zero Ca^{2+} and, following wash, in response to extracellular stimulation (arrow). The plots are averages of four trials, paired-pulse extracellular stimulation, 105 ms interval.

(B) (Left) Averaged fura-2 image indicating 11 axonal sites (1.4 × 1.4 μm area) that were quantified to determine dependence of axonal Ca^{2+} transients on high voltage activated Ca^{2+} channels. Site 8 is closest to the soma. The inset shows sites 1, 2, and 3 at higher magnification. The inset is 15 μm × 20 μm. (Right) Traces of change in $[Ca^{2+}]_i$ versus time in response to paired extracellular stimulation during control (thin lines, average of eight trials) and after combined application of ω-agatoxin IVA (200 nM) plus ω-conotoxin GVIA (1 μM) plus ω-conotoxin MVIIC (1 μM), thick lines, average of 10 trials. (Bottom) Change in $[Ca^{2+}]_i$ averaged over 500 ms poststimulation, for the 11 sites, before and after addition of toxins.

Dependence of Axonal Ca^{2+} Transients on Extracellular Ca^{2+} and on High Voltage–Activated Ca^{2+} Channels

The axonal Ca^{2+} transients were completely abolished in nominally zero extracellular Ca^{2+}; this effect was reversible as shown in Figure 3A, suggesting that the Ca^{2+} transients are due predominantly to Ca^{2+} influx ($n = 5$ cells). Therefore, we examined the effects of high voltage–activated (HVA) Ca^{2+} channel antagonists on the axonal Ca^{2+} transients. We used a combination of three toxins to block the multiple types of HVA channels that have been shown to play a crucial role in synaptic transmission (Takahashi and Momiyama, 1993; Castillo et al., 1994; Wheeler et al., 1994; Dunlap et al., 1995). Combined application of ω-agatoxin IVA (200 nM), ω-conotoxin GVIA (1 μM), and ω-conotoxin MVIIC (1 μM) consistently reduced axonal Ca^{2+} influx at varicosities by 40%–70% in response to action potential stimulation ($n = 5$ cells). Figure 3B illustrates traces of averaged change in $[Ca^{2+}]_i$ in response to pairs of action potentials at 11 axonal sites in one neuron. Ca^{2+} influx was consistently largest at two varicosities that were located more distally from the soma than other sites along the axon (sites 1 and 2); combined application of the toxins reduced Ca^{2+} response on the order of 70% at these varicosities. Although heterogeneity in responsiveness between different axonal sites was observed under control conditions, all sites examined were sensitive to the antagonists.

Stochastic Fluctuations in Evoked Synaptic Activity Measured Postsynaptically Using Ca^{2+} Imaging

The spatial heterogeneity in presynaptic Ca^{2+} transients in response to action potential stimulation (Figures 1B, 2B, and 2C) suggested a mechanism underlying the reported variability in postsynaptic responsiveness (Rosenmund et al., 1993; Hessler et al., 1993). To determine directly whether evoked responsiveness varied both between and within single synapses, we measured local postsynaptic Ca^{2+} changes in response to local presynaptic stimulation. Postsynaptic neurons were filled with fura-2 under whole-cell recording and maintained at a −35 mV holding potential to decrease the Mg^{2+} block of N-methyl-D-aspartate (NMDA) receptors. Figure 4A shows the change in $[Ca^{2+}]_i$ along a small dendritic region for two individual trials in response to a local presynaptic stimulation (single shock) by a microelectrode (electrode indicated by an asterisk in Figure 4B). In trial 4, stimulation resulted in a local Ca^{2+} transient at site 2 while site 1 failed to respond; conversely, in trial 11, site 1 showed a local response to stimulation while site 2 failed to respond. Over 16 trials performed with a suprathreshold stimulus, we determined that the two sites showed markedly different probabilities ($P_{site\ 1} = 0.63$ and $P_{site\ 2} = 0.19$) of a postsynaptic response (defined as being 2 SD above baseline). The responsiveness of the two dendritic sites appeared to be attributed to factors unique to each site since a cross-correlation of the Ca^{2+} transient amplitudes (for the two sites) did not indicate any significant relationship ($r = 0.27$, $p > .05$). The difference in probability between sites was statistically significant as determined by the χ^2 test ($p < .05$).

Inspection of the records of postsynaptic current confirmed that the extracellular stimulation resulted in a synaptic response in every stimulation trial. The average postsynaptic current in the presence and absence of APV is shown in Figure 4B. As there were at least two postsynaptic sites that were responsive to presynaptic stimulation, for each trial responses at sites 1 and 2 were averaged for correlation with synaptic currents. There was a significant correlation between the Ca^{2+} response and the magnitude of the inward synaptic current ($r = 0.64$; $p < .05$; the first 100 ms of the current integrated) for the 16 trials performed in the absence of

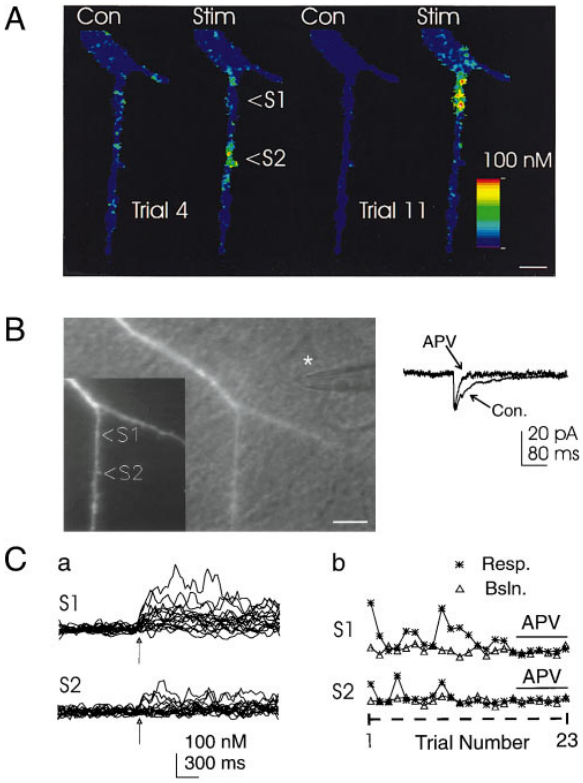

Figure 4. Stochastic Fluctuations in Evoked Synaptic Activity Measured Postsynaptically Using Ca^{2+} Imaging

(A) Images of changes in dendritic $[Ca^{2+}]_i$ averaged over 500 ms before and after extracellular stimulation of presynaptic fibres for trials 4 and 11. Two responsive sites were identified and are indicated by arrowheads. Trial 4, stimulation resulted in a local Ca^{2+} transient at site 2; trial 11, stimulation resulted in a local Ca^{2+} transient at site 1. Scale bar 5 μm. The color scale corresponds to a change in $[Ca^{2+}]_i$ from 0–100 nM; for presentation purposes, a 2 nM threshold increase in Ca^{2+} was applied to the images shown, and a boxcar filter of 2 × 2 pixels was applied to each image.

(B) (Left) Combined bright-field and fluorescence image showing dendrite and position of presynaptic stimulating electrode, indicated by the asterisk. (Inset) Averaged fura-2 image illustrating the sites exhibiting the localized Ca^{2+} responses illustrated in (A). Scale bar 10 μm. (Right) The postsynaptic current recorded following presynaptic stimulation, averaged over 16 trials prior to addition of APV and averaged over 7 trials following addition of APV. The slow component of the EPSC is reduced following addition of APV. The average response in the presence of APV was scaled to the amplitude of the control response. The stimulus artifact was removed for presentation.

(C) (a) Record of change in $[Ca^{2+}]_i$ versus time, superimposed for 16 trials, for sites 1 and 2 in the absence of APV. A single presynaptic stimulation was delivered at the time marked by the arrow. (b) Baseline and stimulated Ca^{2+} response versus trial for sites 1 and 2 over 16 trials before APV addition and 7 trials following APV addition; responses are 500 ms averages.

the NMDA receptor antagonist APV. Application of APV abolished the Ca^{2+} transients and reduced the slow component of the synaptic current response; therefore, the slow NMDA receptor mediated component of the synaptic current appeared to underlie the postsynaptic Ca^{2+} transients.

Figure 4C demonstrates the variability in Ca^{2+} response at sites 1 and 2. Figure 4Ca shows superimposed traces of Ca^{2+} response versus time at sites 1 and 2 for 16 trials. Both sites show a large variability in postsynaptic responsiveness following presynaptic stimulation. In the case of site 1, a statistically significant increase in variance over baseline was observed despite the exclusion of trials that did not result in a significant Ca^{2+} transient ($p < .05$, F test), suggesting that the postsynaptic variability is due to additional factors other than failure of transmission. Significant variability ($p < 0.05$, F test) in postsynaptic evoked activity for the sites discussed above was observed when responses were expressed as a ratio to baseline fluorescence from which values of $[Ca^{2+}]_i$ were calculated (as above and in Figure 4), or if changes in raw fluorescence were fitted to an average response (see Experimental Procedures as in Figure 6). Figure 4Cb plots the magnitude of Ca^{2+} response (averaged over 500 ms) at each site as a function of trial. Trials were observed in which both sites responded (e.g., trial 9), only site 1 responded (e.g., trial 11), or only site 2 responded (e.g., trial 4). Statistically significant heterogeneity in evoked postsynaptic responsiveness was observed in three other neurons that were analyzed. To investigate to what extent variability in the amplitude of the presynaptic Ca^{2+} transient contributed to this observed postsynaptic heterogeneity, we determined the reliability of presynaptic Ca^{2+} influx.

Reliable Coupling between Single Somatic Action Potentials and Elevation in Ca^{2+} at Presumed Presynaptic Release Sites

At presumed neurotransmitter release sites with a relatively high signal-to-noise ratio (>2.5), we examined the reliability of coupling between single action potentials and a rise in Ca^{2+}. Figure 5 (top right) presents records of change in $[Ca^{2+}]_i$ versus time at six sites in response to single action potentials for 30 trials (every third trial overplotted). Sites 3, 4, and 5 each showed a significant increase in variance following single action potential stimulation (data fit as in Figure 6; F test, $p < .05$). Figure 5 (bottom) plots the 500 ms average of the Ca^{2+} response (and of baseline) across the 30 trials for each of the six sites. Although some sites (1, 4, 5, and 6) showed occasional response failures, which we defined as a response within 2 SD of baseline, these failures were relatively uncommon. For example, although site 3 exhibited a high level of response variability, we did not observe failure within 30 trials of single action potentials. In all 71 low noise axonal sites from eight cells examined, we observed 43 response failures in 994 total trials, or 4.3%. Using a fitting procedure described in Figure 6, a similar low level of apparent failures was observed: 15 failures in 709 trials, or 2.1% (50 sites). These failures were not attributed to lack of action potential generation or propagation for two reasons: first, in all cases, action potentials were recorded in current-clamp mode; second, Ca^{2+} responses were observed in the same trial in neighboring distal regions. Conceivably, these apparent failures are due to variation in response due to noise as they were infrequent and usually occurred at the sites with lower signal to noise properties.

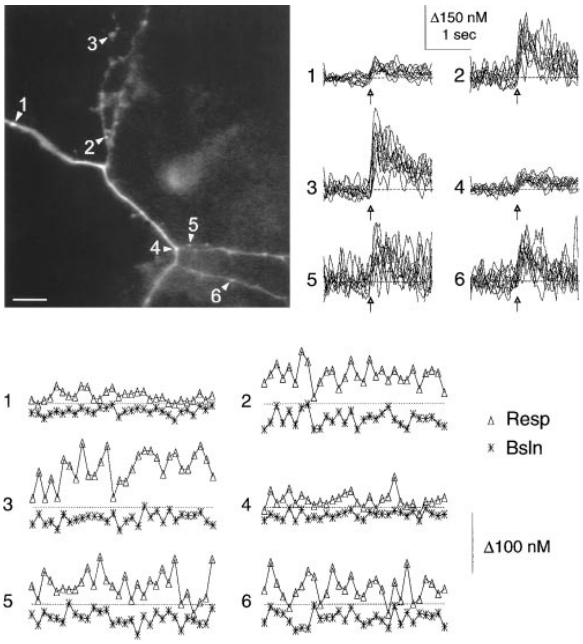

Figure 5. Reliable Coupling of Single Action Potentials to Axonal Ca^{2+} Transients

(Top left) Averaged fura-2 fluorescence image showing six individual numbered axonal sites where responses were quantified (2.4 × 2.4 μm area) over 30 trials. Scale bar 10 μm. (Top right) Records of change in $[Ca^{2+}]_i$ versus time for six individual sites for 30 trials: every third trial is plotted for clarity. (Bottom) Baseline and stimulated axonal Ca^{2+} response (500 ms averages) plotted across 30 trials for the six sites. Dotted lines indicate 2 SDs above baseline (used as a response criterion). Note that raw fluorescence data was converted to $[Ca^{2+}]_i$ to compare Ca^{2+} influx between sites. This procedure will likely exaggerate variability in Ca^{2+} transients across trials (see Experimental Procedures and Figure 6 for variability analysis using raw data).

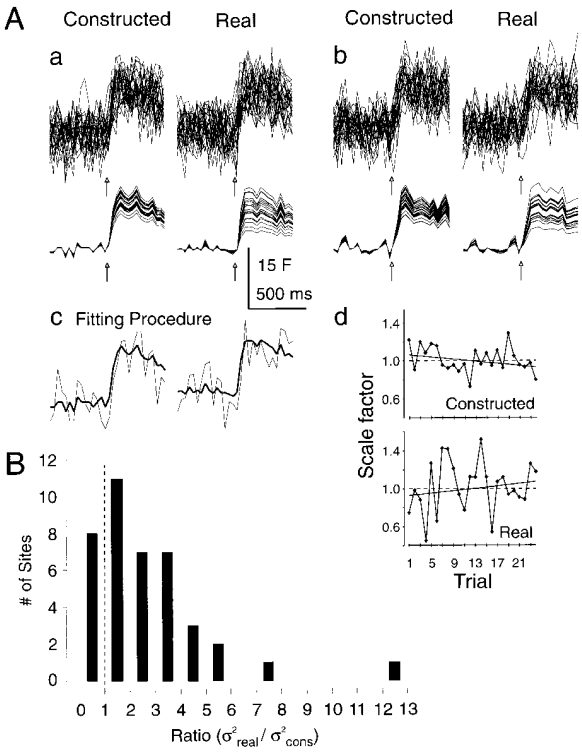

Figure 6. Variation in Presynaptic Ca^{2+} Transients in Response to Single Action Potentials

(A) (a) Constructed and real Ca^{2+} responses to a single action potential from a presumed release site exhibiting significant variability in response. Constructed responses were generated by adding (for each trial) segments of baseline to a mean response. (Top) Records of raw fura-2 fluorescence versus time overplotted for 24 individual trials. The single action potential was delivered at the time indicated by arrow. (Bottom) Overplotted fitted traces (24 trials) for real and constructed data corresponding to the "noisy data" shown above illustrating the variability in the scaled traces. For the purposes of presentation, each trace was offset (<5 raw pixel value) to overlay the baseline periods. (b) Constructed and real Ca^{2+} responses to a single action potential from a presumed release site exhibiting no significant variability of response. Raw fura-2 traces (top); fitted traces (bottom). (c) Illustration of the fitting procedure for a single trial for the site shown in (a). For both the constructed and real responses, the raw trace (thin line) was fitted by multiplying an averaged trace (thick line) by a scaling factor (real data on right). (d) Scale factor versus trial for constructed and real data for the site shown in (a); each point represents the magnitude of the amplitude scaling factor used to fit the average curve to the raw curve for a given trial. The dotted line illustrates the average scale factor (1.0); the solid line illustrates the slope of the regression versus trial, illustrating possible run up or run down over time. For this site, the CV_{real} was 26.9% and the CV_{cons} was 13.6%; subtraction of variance due to steady state changes (estimated by regression) did not greatly alter these values (CV_{real} = 26.5%, CV_{bsln} = 13.0%).

(B) Frequency distribution of the ratio of the variance of the real data divided by the variance of the constructed data ($\sigma^2_{real}/\sigma^2_{cons}$) for the 40 putative release sites examined from 5 cells using fura-2 (583 total trials of single action potentials). A ratio = 1 represents no difference in variance between real and constructed traces for a given site; a ratio > 1 represents increased variance in the real data compared to baseline (constructed) data. The mean ratio was equal to 2.7 and the median was 2.3; 32 of 40 sites had a ratio > 1.

Variation in Presynaptic Ca^{2+} Transients in Response to Single Action Potentials

Initial experiments suggested that variability in presynaptic Ca^{2+} transients during evoked synaptic transmission was small compared with the variability we measured postsynaptically (in dendrites, see Figure 4) and could be occluded by the high baseline noise. Therefore, we confined analysis to experiments and axonal sites with the highest signal-to-noise properties (ratio > 2.5). Variability in responsiveness was evaluated separately for each site by comparing the variance in baseline before stimulation to the variance in response after action potential stimulation. For each trial, we constructed simulated responses (with baseline variance) by adding the average Ca^{2+} transient for that site to a baseline period for that trial (Figure 6A). We then compared the variability in the constructed (baseline) data to the variability of the real (response to stimulation) data using a curve fitting procedure. The actual responses and the constructed responses were fitted by scaling the averaged Ca^{2+} transient (Figure 6Ac, thick trace) using an amplitude scaling factor. The amplitude scaling factor was a measure of the difference of each curve (corresponding to a single trial) from the mean response; for example, a scaling factor of 1.0 meant that a particular trial had an amplitude that was identical to the mean. A CV for the scaling factors was calculated by dividing the SD of the scaling factors by the mean scaling factor (mean

scaling factor = 1.0). The CV of the constructed response scaling factors (CV_{cons}), a measurement of the variability due to baseline noise alone, averaged 19%, indicating a relatively high signal-to-noise ratio ($\sim$5 as 100%/CV_{cons} = signal to noise). Scaling factors for actual (real) response trials were compared to constructed responses using an F test. Figures 6Aa and 6Ab illustrates traces of raw fura-2 fluorescence (above) and traces of fitted average responses (below) for both constructed and real data. For the records from the presumed release site shown in Figure 6Aa, the amplitude scaling factors were significantly more varied for the real responses than for the constructed responses. For the release site illustrated in Figure 6Ab, there was no significant difference in the variance of the amplitude scaling factors between real and constructed responses by individual F test. Examination of all low noise presumed release sites imaged with fura-2 indicated that for 12 of 40 sites (30%; 5 cells) the actual scaling factors were significantly more varied than the constructed scaling factors ($p < .05$; F test); none of the 40 sites showed a statistically significant decrease. Since the level of significance was set at .05, 2 of the 12 significant observations could have been spurious.

Although 12 of 40 sites showed individual significance by F test, at sites that lacked significance we observed that scaling factors for real data were often more varied than constructed data (see example in Figure 6Ab), suggesting that a larger proportion of boutons may show varying responses. To better evaluate variability at individual boutons, we constructed a histogram of variance ratios to express the variance of the real data as a proportion of the variance of the constructed data ($\sigma^2_{real}/\sigma^2_{cons}$; σ is the SD of the scaling factors) for each of 40 putative release sites examined (Figure 6B). If there was no consistent difference between the real and the constructed baseline variance, the mean of the distribution should be 1 with an equal number of observations greater than and less than 1. In contrast, we observed a skewed distribution with a mean of 2.7, a median of 2.3, and 32 of 40 observations greater than 1. A t test indicated that the mean of the distribution was significantly different from 1 ($p < .0001$). The significance by t test was not merely due to the 12 of 40 sites that showed significantly greater variability in σ^2_{real} than σ^2_{cons} by individual F test, since exclusion of these values resulted in a mean ratio of 1.7 ($\sigma^2_{real}/\sigma^2_{cons}$), which was also significantly different from a mean of 1 ($p < .001$). A second method used to analyze the distribution of variance ratios was to convert the variance ratio at each site to a percentile of its F distribution (the entire population could not be fitted to a single distribution because of uneven trial numbers between cells). From the distribution of the percentiles, we found the median percentile score was 0.91. That is, 50% of the sites had a variance ratio in the upper 9% of the F distribution, which was unlikely to have occurred by chance (χ^2, $p < .00001$). After exclusion of the individually significant sites (by F test), the nonsignificant sites had a median percentile score of 0.78, which was also significant by χ^2 ($p < .00005$). Thus, although not significant by individual F test, analysis of group data on these sites indicates significantly greater variability in σ^2_{real} than σ^2_{cons} that cannot be attributed to random behavior. The lack of significance using the F test at some sites (28 of 40) could be due to the relatively low number of trials and to high noise levels compared with the small increase in variance associated with single action potentials (Zar, 1984). Consistent with the distribution analysis, when the 40 presumed release sites were examined together, the average CV_{cons} for baseline constructed responses was smaller than the average CV_{real} attributed to actual responses (average $\pm$ SD; CV_{cons}, 18% $\pm$ 5%; CV_{real}, 26% $\pm$ 9%; $p < .00001$, F test). As the CV of the actual responses reflects both baseline and Ca^{2+} transient variability, we assumed that the variability attributed to baseline (estimated from constructed responses) and the variability attributed to Ca^{2+} transients were additive by the equation:

$$CV_{real} = \text{Sqrt}\,(CV_{cons}^2 + CV_{Ca^{2+}}^2) \quad (1)$$

Solving the equation for CV_{Ca}^{2+} indicated that the Ca^{2+} transient in the absence of baseline variation would on average have a CV of 19%. Thus, results using fura-2 indicate that variability in the magnitude of the presynaptic Ca^{2+} transient due to single action potentials is on average low, but consistently above that attributed to baseline alone. As F tests on individual boutons indicated that some sites had significantly greater variability in Ca^{2+} transients than others, it is possible that these sites may constitute a subpopulation of more variable sites. In this scenario, the 12 of 40 sites (30%) that showed significantly greater σ^2_{real} than σ^2_{cons} have a CV_{Ca}^{2+} of 29%, while the remaining sites, that as a group show significance, have a CV_{Ca}^{2+} of 13%.

Apparent variability in the presynaptic Ca^{2+} transient was not attributed to a consistent run down or run up of responsiveness over trials as boutons that showed a significant time-dependent change in response ($p < .05$) were excluded from analysis (see Experimental Procedures and Figure 6Ad). For the remaining sites with a poor correlation with trial number ($p > .05$), an unpaired t test revealed no significant difference between constructed and real data in the average slope derived from linear regression analysis. This indicated that any potential error was probably due to random factors and would affect CV_{real} and CV_{cons} equally. Furthermore, the error was small and was estimated to account for less than 5% of CV_{real} and CV_{cons} (see Figure 6Ad). Therefore, steady changes in responsiveness could not account for the observation that σ^2_{real} was significantly greater than σ^2_{cons} (Figure 6B). As an additional test, in two representative cells, we examined whether the amplitude scaling factors (for the Ca^{2+} responses) were significantly correlated between different axonal sites within the same cell across trials of action potentials (144 total pairwise comparisons). In only 8 of 144 cases did we observe a significant correlation ($p < .05$), suggesting that the observed variability in scaling factors was unique to each site and presumably not attributed to changes in recording conditions or action potential propagation (see examples in Figure 5). The low degree of correlated activity between sites is likely spurious as constructed data sets also showed a small number of significant correlations (4 of 144 pairwise comparisons).

Discussion

Local Domains of Ca^{2+} Influx at Neurotransmitter Release Sites

Using fluorescence microscopy on cultures of cortical neurons, in which light scattering due to out of focus fluorescence is minimal, we have been able to trace the axon of a mammalian central neuron from the soma to distal release sites on collateral branches. Measurement of Ca^{2+} influx in response to single action potentials indicated that axonal varicosities have enhanced Ca^{2+} influx when compared with the large main branches of the axon or the segments of axon collaterals that occur between release sites (Figures 1A, 2A, 2B, and 5). Conceivably, this could be due to differences in surface area-to-volume ratio of the regions imaged (Smith et al., 1993). However, when sites along collateral branches were compared, we observed that varicosities, which had higher fura-2 fluorescence and presumably larger volume, showed larger responses than neighboring regions of similar or smaller volume (Figures 1B, 2A, 2B, 2C, and 3B), arguing against hot spots of Ca^{2+} elevation due merely to surface-to-volume ratio. The presence of release sites at these varicosities was determined morphologically at both the light and electron microscopic level. Although we could identify the release sites, we could not determine whether some axonal varicosities contained multiple release sites (Harris, 1995). Subcellular fractionation studies and immunocytochemistry suggest that there are mechanisms to concentrate the machinery for neurotransmitter release at *en passant* synapses selectively (Sheng et al., 1994). Furthermore, theory and experimental observations suggest that there should be a close correspondence between presynaptic Ca^{2+} channels and release sites (Pumplin et al., 1981; Adler et al., 1991; Zucker, 1993). Our study indicates that the function of voltage-gated Ca^{2+} channels is enhanced at the sites of neurotransmitter release and suggests that Ca^{2+} channels may fall into the same category as proteins of the release apparatus that undergo selective targeting. Although the axonal Ca^{2+} transient was enhanced at release sites, changes in Ca^{2+} concentration also occurred along the segment of axon between sites of neurotransmitter release (Figures 2A and 2B). In the dendritic experiments (Figure 4A), evoked postsynaptic Ca^{2+} transients diffused from a point source; in contrast in the axon, Ca^{2+} concentration between varicosities increased too rapidly and homogeneously to have spread from sources at nearby varicosites, suggesting that Ca^{2+} channels must be located along the intervening segments. Conceivably, Ca^{2+} channels at sites other than release sites could function in the propagation or regulation of the action potential, or processes such as axonal transport. Our findings in *en passant* central synapses are consistent with reports from invertebrate neuromuscular junction and sympathetic neurons in which increased Ca^{2+} channel function at nerve terminal arborizations have been observed (Smith and Augustine, 1988; Robitaille et al., 1990; Smith et al., 1993; Delaney et al., 1991; Toth et al., 1993; Cooper et al., 1995). Unlike these previous studies, we demonstrate the concentration of Ca^{2+} channel function at *en passant* presynaptic elements that occur in the mammalian CNS and are involved in forms of activity dependent plasticity (Sorra and Harris, 1993; Harris, 1995).

The observed overlap of sites of functional vesicular turnover and sites of enhanced Ca^{2+} influx supports previous studies that have used FM1-43 as a marker for functional presynaptic terminals (Betz and Bewick, 1992; Ryan and Smith, 1995; Reuter, 1995; Liu and Tsien, 1995). These studies have also shown overlap between FM1-43 uptake and presynaptic markers such as synapsin 1 (Betz and Bewick, 1992; Ryan et al., 1993). In some experiments, we did observe axonal varicosites that showed localized Ca^{2+} transients yet failed to take up FM1-43 in response to a short train of action potentials (data not shown). This observation raises the possibility that factors other than Ca^{2+} influx regulate vesicular turnover, consistent with the recent study of Malgaroli et al. (1995). However, owing to complicating factors such as a poor signal to noise in the FM1-43 uptake experiments (due to apparent diffuse glial uptake) and the possibility that fura-2 may buffer rises in intracellular Ca^{2+} and reduce vesicular turnover (at some synapses), we are cautious in concluding that differential uptake of FM1-43 occurs in our system (Betz and Bewick, 1993). However, despite these caveats, our results indicate that vesicular turnover and apparent neurotransmitter release can occur under the conditions of our imaging experiments, as evidenced by the specific loading and unloading of boutons labeled with FM1-43.

Local Variability in Evoked Postsynaptic Ca^{2+} Transients

Synaptic transmission occurring at individual mammalian CNS synapses is an unreliable process, as evoked synaptic stimulation often fails (del Castillo and Katz, 1954; Malinow and Tsien, 1990; Stevens and Wang, 1994; Malinow, 1994). Previous studies have used Ca^{2+} imaging postsynaptically to evaluate the reliability of evoked synaptic transmission (Malinow et al., 1994; Yuste and Denk, 1995). These studies observed stochastic failures (Yuste and Denk, 1995) and apparent differences in response probability between synapses (Malinow et al., 1994). However, these studies were limited in that it was not possible to resolve multiple postsynaptic sites simultaneously (Yuste and Denk, 1995) and in some cases involved multiple presynaptic stimuli (Malinow et al., 1994). Using a similar postsynaptic imaging approach, we have extended these studies by observing differences in responsiveness, including failure, between adjacent synaptic sites on the same dendritic branch. Our studies directly demonstrate selective regulation of response probability with single presynaptic stimuli. Analysis of the current records indicated that each stimulus resulted in a postsynaptic response, suggesting that the differences were not due to failure to generate an action potential. However, we cannot exclude the possibility that the synapses we observed were innervated by two different axons with different thresholds for action potential generation. The relatively high signal-to-noise ratio of our images allowed us to demonstrate variability in the evoked response despite

the exclusion of trials in which failures occurred, consistent with imaging of miniature synaptic activity and recordings of postsynaptic currents elicited at single boutons (Murphy et al., 1995; Liu and Tsien, 1995).

Reliable Conduction through Axonal Arbors

Imaging of axonal arbors indicated that virtually every action potential generated at the cell soma penetrates even distal collateral branches to result in a Ca^{2+} transient at all presumed release sites. These results indicated that failure of axonal conduction is not a source of unreliability in CNS evoked synaptic transmission. Our direct imaging of the axon extends previous studies of paired-pulse facilitation that demonstrated that even if the first response fails paired-pulse facilitation still occurs (Stevens and Wang, 1995) with the observation that this reliability in the Ca^{2+} transient occurs at all boutons. In some experiments when baseline noise levels were high (30%–60% CV; noise not attributed to stimulation), we observed that some axonal sites appeared to show frequent failures ($\sim$50%) in response to action potential stimulation. Conceivably, these apparent failures were due to overlap between the distribution of the noise and the responses to single action potentials. When cells with higher signal to noise were analyzed, we observed that single action potentials produced a rise in $[Ca^{2+}]_i$ 2 SDs above baseline in 96% of trials (see Results and Figure 5), indicating reliable coupling between single action potentials and presynaptic Ca^{2+} transients. Although failures were rare with single action potentials, with high frequency stimulation we observed saturation of the presynaptic Ca^{2+} response with increasing numbers of action potentials (1, 2, 3, and 4; see Figure 1A). Nonlinearity in axonal Ca^{2+} responses to paired-pulse stimulation has been previously described (Wu and Saggau, 1994c); however, this effect may be due to saturation of fura-2 in response to trains of action potentials (Regehr and Atluri, 1995). We are currently in the process of comparing axon collaterals to main branches to determine whether distal branches are more likely to exhibit frequency dependent response failure. Branch-point failure has been reported for both axonal and dendritic action potential conduction (Lüscher et al, 1994; Wall, 1995; Spruston et al., 1995).

Variability in Presynaptic Ca^{2+} Transients at Individual Release Sites and Implications for Release Probability

By capturing relatively low noise images of Ca^{2+} influx into the axons of cultured cortical neurons, we observed that most release sites undergo a stereotyped, relatively constant increase in Ca^{2+} levels in response to single action potentials. Using a fitting procedure, we estimated that variability in the presynaptic Ca^{2+} transient was in the of range of 15%–20% (Figure 6 and Results). Although the variability associated with presynaptic Ca^{2+} transients was small, several observations indicated that this variability was not due to factors associated with the detection of fluorescence (for discussion see Experimental Procedures). Furthermore, the variability observed with fura-2 does not appear to be an underestimate due to possible saturation of fura-2 (Regehr and Atluri, 1995), as preliminary experiments with fluo-3, a lower affinity probe, indicate a similar low level of variability in the range of 15% (3 cells, 5 boutons; data not shown). At synapses that did show a significant amount of Ca^{2+} transient amplitude variability, we determined whether the source of fluctuations in $[Ca^{2+}]_i$ transient amplitude was due to factors common to all synaptic sites by correlating the amplitudes of different sites along the same axon across trials (see results). Significant correlations between sites were rare and sites in which the amplitude of the Ca^{2+} transient correlated with trial number were excluded from the analysis, suggesting that the variability at a given site was due to properties unique to each site. Thus, Ca^{2+} transient variability at a single release site could be due to stochastic properties of a small number of Ca^{2+} channels opening as a consequence of a single action potential (Pumplin et al., 1981; Smith and Augustine, 1988). If Poisson statistics are assumed, a CV of 15%–20% could be attributed to the stochastic properties associated with the opening of $\sim$50 presynaptic Ca^{2+} channels at a single release site (Hille, 1992). Alternatively, moment to moment changes in a biochemical process such as phosphorylation or G protein modulation could lead to variability in Ca^{2+} response at a single axonal site. Although variability in the presynaptic Ca^{2+} transient was low ($\sim$15%–20%), it would be sufficient to affect synaptic transmission given the suggested power relationship between Ca^{2+} influx and transmitter release (Dodge and Rahamimoff, 1967; Augustine and Charlton, 1986; Heidelberger et al., 1994; Mintz et al., 1995).

To evaluate the extent to which small changes in presynaptic Ca^{2+} transient amplitude could affect transmitter release, we calculated the range of postsynaptic responses expected for 10% variability in the presynaptic Ca^{2+} transient for a linear and fourth power relationship between Ca^{2+} influx and neurotransmitter release. In the case of a fourth power law, a 10% variation in the presynaptic Ca^{2+} transient would lead to a postsynaptic response that varied by up to 35%. Measurements of variability in postsynaptic evoked responses range from $\sim$20% (Jonas et al., 1993) to $\sim$50% (for this system, see Figure 4; Bekkers and Stevens, 1990; Raastad et al., 1992; Volgushev et al., 1995). These results indicate that a small amount of variability in the presynaptic Ca^{2+} transient could contribute to the observed variability in postsynaptic responsiveness. However, variability in postsynaptic responses is not likely to be entirely controlled at the level of the presynaptic Ca^{2+} transient, as miniature synaptic currents recorded from a single synapse can also vary in amplitude (Murphy et al., 1995; Frerking et al., 1995; Liu and Tsien, 1995). Furthermore, Ca^{2+} transients measured with high affinity probes over a relatively large volume (as we have done) reflect the amount of Ca^{2+} that enters the terminal and not necessarily the flux that triggers transmitter release. Although a 3–4 power relationship between Ca^{2+} entry and release would suggest that small changes in the number of Ca^{2+} channels would have a large effect on neurotransmitter release, it is also possible that the observed small fluctuations in Ca^{2+} transients reflect the recruitment of channels that do not interact cooperatively to induce transmitter release. This scenario would lead to a linear

relationship between the observed fluctuations and release, as cooperativity between Ca^{2+} channels is required to observe a power relationship between Ca^{2+} and transmitter release (Mintz et al., 1995; Augustine et al., 1990). Nevertheless, our experiments suggest that the coupling of somatic action potentials to distal functional release sites is a reliable process, as virtually all action potentials produce an elevation in Ca^{2+} within ~70%–80% of maximal values. The existence of a relatively heterogeneous complement of Ca^{2+} channels (assayed by influx) between synapses (Figure 1; Reuter 1995; Cooper et al., 1995) and the low but consistent level of variability at a single synapse (Figure 6) suggest fruitful future experiments in which the relationship between presynaptic Ca^{2+} dynamics and release are simultaneously measured at a single synapse.

Experimental Procedures

Cortical neurons and glia were dissociated from rat fetuses (17–18 day gestation), placed in culture, and allowed to mature for 17–26 days in vitro as previously described (Murphy and Baraban, 1990), with the exception that the plating medium L-cystine concentration was supplemented to 300 μM. In all experiments, the whole-cell recording configuration (Hamill et al., 1981) was used to fill neurons with fura-2 or fluo-3/Mag-fura (Minta et al., 1989; Ragu et al., 1989). The patch pipette solution contained 0.75–1.0 mM fura-2 K^+ salt (Grynkiewicz et al., 1985), 140 mM K^+ $MeSO_4$, 5 mM Mg-ATP, 0.3 GTP, 10 mM NaCl, and 10 mM HEPES (pH 7.2). In experiments using fluo-3, 750 μM K^+ salt was used in combination with 500 μM Mag-fura (Mag-fura used to view basal fluorescence). Imaging was performed with a 63× water immersion Zeiss objective on a movable upright Zeiss Axioskop microscope. The current-clamp recording method was used for all experiments done with the upright microscope. Resting membrane potential typically ranged from −50 to −60 mV. Membrane potential was adjusted to −60 mV by injection of a small negative or positive current, and overshooting action potentials were produced by injection of positive current (5 ms duration). In all trials of action potentials, records of membrane potential were inspected carefully to determine whether the action potential changed shape over time or whether stimulation failed. Cells that fired more than one action potential during a 5 ms current injection were not analyzed. Experiments were terminated if a progressive change in the action potential shape occurred, or if resting membrane potential changed by more than 10 mV. Experiments involving higher resolution axonal imaging (as indicated) were performed on a Axiovert inverted microscope using a Zeiss 100× oil 1.3 NA objective. Fura-2 loading with this system was performed under the whole-cell recording mode using patch-clamp pipettes (~10–12 MΩ, containing 5–10 mM fura-2, 150 mM KCl, and 10 mM HEPES). After the neurons were loaded (~2 min of perfusion), patch-clamp pipettes were removed and the cells were allowed to recover in the presence of TTX for about 1–2 hr (Murphy et al., 1995). Calibration parameters for fura-2 were determined in vitro. Using intracellular perfusion with known amounts of fura-2, we estimated that 750–1000 μM fura-2 approximates the amount microinjected. The axon of the neuron was identified (see Results) and positioned in the center of the video field. Extracellular stimulation with a ~2–4 MΩ patch pipette filled with bathing solution and positioned over the cell body but not in contact with the cell (usually near the origin of the axon) was used elicit action potentials. The stimulus parameters were 0.2 ms and 10–90 V. The stimulus voltage varied considerably between different cells and electrodes and was presumably due to distance from the neuron or the electrode characteristics. For a given cell, a threshold was estimated and the stimulus voltage was adjusted so it was typically 50% above threshold. Experiments with extracellular stimulation were terminated if threshold increased by more than 50% during an experiment or if a rise in resting $[Ca^{2+}]_i$ occurred. Once threshold was exceeded increases in stimulation did not result in a further rise in the presynaptic Ca^{2+} transient, indicating that it is an all or none phenomenon (data not shown). The following extracellular solution was used to isolate the effects of action potential stimulation from spontaneous synaptic activity (Murphy et al., 1994) 137 mM NaCl, 5.0 mM KCl, 2.5 mM $CaCl_2$, 1 mM $MgCl_2$, 0.34 mM $Na_2HPO_4(7H_2O)$, 10 mM Na-HEPES, 1 mM $NaHCO_3$, 0.01–0.1 mM picrotoxin, 100 μM APV, 3 μM CNQX, and 22 mM glucose (pH 7.4 and ~320 mOsm). Cells were switched to this solution at least 10 min before imaging. With the exception of the data in Figure 5 and the example in Figure 6 (which used 5 mM $CaCl_2$ and was not noticeably different from other experiments), all experiments used 2.5 mM extracellular $CaCl_2$.

For experiments in which the postsynaptic effects of evoked responses were measured, CNQX and APV were omitted from the recording medium and 10–20 nM TTX was added to the bath to block polysynaptic evoked activity and to suppress spontaneous activity (Fields et al., 1991). The patch pipette solution for these experiments contained 0.5–0.75 mM fura-2 K^+ salt, 126.0 mM $CsMeSO_4$, 5.0 mM Mg-ATP, 0.3 mM GTP, 1.0 mM QX-314, 10.0 mM KCl, and 10.0 mM HEPES (pH 7.2). For simultaneous measurements of synaptic currents and evoked dendritic Ca^{2+} transients, we used a Zeiss 100×, 1.3 numerical aperture objective and positioned the cell body of a fura-2-filled neuron at the edge of the microscopic field so that the dendritic field was visible in the video field. Extracellular presynaptic stimulation was performed as described above.

FM1-43 Imaging

FM1-43 recycling was performed as described by Reuter (1995) with the exception that, in order to avoid background uptake, action potentials used to stimulate exocytosis were delivered only to the cell that was also imaged using fura-2. Fura-2 and FM1-43 fluorescence were measured in the same neuron by alternating between 380 nm (fura-2) and 490 nm (FM1-43) excitation filters with the use of a 535/40 band-pass filter and a combined fluorescein/fura-2 dichroic mirror (Chromo Technologies). Using this configuration, no fura-2 signal was detected at gain settings and filter combinations used to detect FM1-43 fluorescence. For presentation purposes, FM1-43 images were reversed (negative) and subjected to a pixel threshold.

Imaging and Analysis

A fiberoptically coupled intensified CCD camera with a Gen III intensifier tube was used for all experiments (Stanford Photonics, Palo Alto, CA) in combination with an Epix 4M12-64 MB frame grabber board. Images and electrophysiological data were analyzed together on a Pentium 90 MHz microcomputer using custom routines written in the program IDL (Research Systems, Incorporated). Plots of $[Ca^{2+}]_i$ versus time were produced off-line, either from single video frames (30/s) or three frame averages as indicated (see figures). Following analysis, data was discarded if basal Ca^{2+} levels were found to significantly rise during the course of an experiment or if we observed progressive changes in the amplitude of $[Ca^{2+}]_i$ attributed to factors such as spike broadening. Since the evoked synaptic currents have slow components (that were attributed to the rises in Ca^{2+}), the first 100 ms of a synaptic current was averaged for correlation with evoked Ca^{2+} transients. To improve the signal-to-noise ratio for Ca^{2+} transients, we averaged the first 500 ms of the Ca^{2+} transient in response to presynaptic or action potential stimulation (in fluo-3 experiments, the first 333 ms was used). Comparison of Ca^{2+} transients between different regions of dendrite or axon was performed on background-subtracted 380 nm excitation fura-2 fluorescence in which values were divided by a 0.5 s baseline period (F_o) that preceded action potential or presynaptic stimulation (expressed as F/F_o*100). Although statistical comparisons were made on changes in raw fluorescence values, these values were converted to a change in $[Ca^{2+}]_i$ using a 380 nm excitation self-ratio for presentation by conservatively assuming a resting Ca^{2+} level of zero and by using the following equation (K_D assumed to be 200 nM):

$$(1 - F/F_0)/(F/F_o - F_{maxCa}/F_{minCa})*K_D.$$

Calculation of $[Ca^{2+}]_i$ by ratio to the isobestic point of fura-2 (360 nm) indicated that with 750 μM K^+ fura-2, the $[Ca^{2+}]_i$ approached zero resting levels (values usually below 40 nM). These low resting

levels were conceivably due to buffering by the relatively high concentration of fura-2 and suggested that the assumptions of the self-ratio were valid. Owing to the characteristics of the objective and light path used (which had relatively poor 360 nm light intensity), we found images produced by 380 nm/360 nm ratio to be less accurate than a 380 nm fura-2 self-ratio.

Analysis of Variability in Presynaptic Ca^{2+} Transients

Statistical testing was performed on the raw data to avoid small artifactual increases in variance due to expressing data as a fluorescence ratio (F/F_o*100). Variance in Ca^{2+} transients was determined using a fitting procedure in which an averaged Ca^{2+} transient (for a particular release site) was scaled by a multiplication factor (a baseline offset constant was also used) for optimal fit to single "noisy" response trials (using routines in Microcal Origin). This procedure was repeated for constructed responses that were generated by adding averaged responses to baseline periods, creating data with defined variance (that of baseline only for comparison). The scaling factors required for best fit of the averaged data to the noisy responses were compared by F test as described in the Results. The fitting analysis was performed prior to any nonlinear scaling of signals (to account for saturation of fura-2 with Ca^{2+}). This was a necessary precaution in order to avoid artifactual increases in noise due to nonlinear scaling of fluorescence changes to $[Ca^{2+}]_i$ as fura-2 approached saturation. This error tended to underestimate rather than account for changes in $[Ca^{2+}]_i$ due to saturation of fura-2, although it was likely to be minimal due to the relatively small changes in $[Ca^{2+}]_i$. Although each cell was carefully examined for time dependent changes in total fluorescence, resting $[Ca^{2+}]_i$, and action potential properties, it was possible that significant run down or run up of responsiveness could account for the variability we observed. Therefore, we excluded any axonal sites that showed potentially time dependent changes in Ca^{2+} transient amplitude. This was accomplished by performing a linear regression analysis on amplitude scaling factors versus trial number for each site. Sites that showed a significant negative or positive correlation ($p < .05$) with trial number were excluded from the analysis even though these changes were local to each bouton, were observed in both real and constructed data, and within the same cell varied in the sign of the slope. For a total of 50 sites examined (100 regression analyses for both the actual and constructed data sets), 10 showed a significant correlation. For the remaining sites, examination of the slopes derived from linear regression of the scaling factors versus trial number (40 sites correlations all $p > .05$) indicated that no consistent negative or positive correlation was apparent as slopes derived for real and constructed values were not significantly different by unpaired t test ($p < .05$).

Potential Sources of Error in Variance of Presynaptic Ca^{2+} Transients

To investigate whether there were potentially artifactual sources of variance associated with measurement of presynaptic Ca^{2+} transients, we determined whether our CCD detection system became more noisy in response to the changes in light levels associated with the fura-2 signal attributed to single action potentials. In contrast with the increase in the variance (of raw fluorescence changes) observed between action potential stimulus trials compared to the baseline, we observed a small but significant decrease in variance due to a 15% reduction in light levels that was comparable to the observed fura-2 fluorescence changes (pixel value SDs: 1.11 to 0.98, $n = 200$, $p < .05$). To obtain these values, light levels were adjusted with a stabilized DC power supply to match those present during an experiment (similar results were obtained by reducing fluorescent light levels with a neutral density filter). Detection system noise was examined at various levels of light, in order to predict the level of noise at a given pixel value (proportional to the square root of the pixel value plus a constant amount of dark noise). This decrease in variance associated with the detection system and the properties of light would cause us to slightly underestimate, rather than account for, the increase of variability associated with single action potentials (using fura-2). In the case of preliminary data using fluo-3, the increased variability associated with action potential stimulation was significantly higher than that attributed to light noise alone (fluo-3 fluorescence increases with $[Ca^{2+}]_i$). As changes in detector noise were small and could not account for the observed increases in variance following action potential stimulation, we did not attempt to correct data to account for this error. Other sources of noise such as fluorescence lamp flickering were minimal (for the experiments and trials analyzed) compared with camera noise, as judged by performing cross-correlations between different regions of background fluorescence. In a few experiments, arc lamp flickers were observed in the occasional stimulus trial; these flickers resulted in obvious highly correlated increases in fluorescence intensity at all sites. Rather than attempt to correct for these events (which may in itself introduce noise), we removed these trials from the analysis.

Electron Microscopy

During recording, selected neurons were perfused with 0.24 mg/ml biocytin and 8 mg/ml neurobiotin. Cultures were then fixed with 4% paraformaldehyde and 0.2%–0.5% glutaraldehyde in 0.1 M Sörensen's Na^+ phosphate buffer (pH 7.2–7.4, 1.5 hr, at room temperature), rinsed briefly in Dulbecco's phosphate-buffered saline (DPBS), permeabilized in 0.2% Triton X-100 in DPBS (4 min, at room temperature), washed with DPBS (3–5 vol over 5 min, at room temperature), and blocked in 2.5% normal goat serum in DPBS (4–12 hr, at 4°C). Cultures were washed with DPBS (3–5 vol over 15 min, at room temperature), incubated with Vector Labs A/B reagent (avidin/biotinylated peroxidase complex) (30 min to 1 hr, at room temperature), washed with DPBS (3–5 vol over 30 min, at room temperature), and then incubated in 0.5 mg/ml diaminobenzidine (DAB) plus 0.015% H_2O_2 in DPBS plus 0.025% $NiCl_2$ (5–20 min, at room temperature, intensity monitored to prevent overstaining). Extensive DPBS washing (5 vol over at least 30 min, at room temperature) was followed by further fixation in 2.5% glutaraldehyde in 0.1 M Sörensen's Na^+ phosphate buffer (pH 7.2–7.4, 1 hr, on ice), washing in the same buffer (3 vol over 30 min, on ice), storage overnight in fresh buffer (4°C), and then postfixation in 1% OsO_4 in the same buffer (1 hr, on ice). Following a final buffer wash (3 vol over 30 min, on ice), cultures were dehydrated in a graded ethanol series (50%, 70%, 85%, 95%, 100%) and flat embedded in Spurr resin on Aclar plastic. Following polymerization, areas containing single stained neurons were excised, separated from the Aclar, and mounted on blank blocks. Serial sections of ~70 nm thickness were collected on Formvar-coated single slot grids, stained with 2%–3% aqueous uranyl acetate followed by Reynold's lead citrate (Reynolds, 1963), and then examined at 80 kV in a Zeiss EM 10C STEM.

Acknowledgments

Correspondence should be addressed to T. H. M. We would like to thank Lynn Raymond, Steve Duffy, and Tony Stea for helpful comments on this manuscript, Gil Weir (University of Maryland) for imaging software, Gail Kenner for preparing EM samples and technical assistance, and Kerry Delaney and David Quastel for helpful discussions. This work was supported by grants from the Medical Research Council of Canada, the Savoy Foundation for Epilepsy, and the British Columbia Health Research Fund to T. H. M.; T. H. M. is an Alfred P. Sloan, EJLB, and Medical Research Council Scholar. P. J. M. is supported by an Medical Research Council studentship.

The costs of publication of this article were defrayed in part by the payment of page charges. This article must therefore be hereby marked *"advertisement"* in accordance with 18 USC Section 1734 solely to indicate this fact.

Received October 11, 1995; revised January 22, 1996.

References

Adler, E.M., Augustine, G.J., Duffy, S.N., and Charlton, M.P. (1991). Alien intracellular calcium chelators attenuate neurotransmitter release at the squid giant synapse. J. Neurosci. *11*, 1496–1507.

Allen, C., and Stevens, C.F. (1994). An evaluation of causes for unreliability of synaptic transmission. Proc. Natl. Acad. Sci. USA *91*, 10380–10383.

Augustine, G.J., and Charlton, M.P. (1986). Calcium dependence of

presynaptic calcium current and post-synaptic response at the squid giant synapse. J. Physiol. (Lond.) *381*, 619–640.

Augustine, G.J., Adler, E.M., and Charlton, M.P. (1990). The calcium signal for neurotransmitter secretion from presynaptic nerve terminals. In Calcium Entry and Action at the Presynaptic Nerve Terminal, E.F. Stanley, M.C. Nowycky, and D.J. Triggle, eds. (New York: New York Academy of Sciences), pp. 365–381.

Bekkers, J.M., and Stevens, C.F. (1990). Presynaptic mechanism for long term potentiation in the hippocampus. Nature *346*, 724–729.

Betz, W.J., and Bewick, G.S. (1992). Optical analysis of synaptic vesicle recycling at the frog neuromuscular junction. Science *255*, 200–203.

Betz, W.J., and Bewick, G.S. (1993). Optical monitoring of transmitter release and synaptic vesicle recycling at the frog neuromuscular junction. J. Physiol. (Lond.) *460*, 287–309.

Cajal, R. (1911). Histology of the Nervous System, N. Swanson and L.W. Swanson, trans. (New York: Oxford University Press).

Castillo, P.E., Weisskopf, M.G., and Nicoll, R.A. (1994). The role of Ca^{2+} channels in hippocampal mossy fiber synaptic transmission and long-term potentiation. Neuron *12*, 261–269.

Cooper, R.L., Martin, L., and Atwood, H.L. (1995). Synaptic differentiation of a single motor neuron: conjoint definition of transmitter release, presynaptic calcium signals, and ultrastructure. J. Neurosci. *15*, 4209–4222.

Delaney, K., Tank, D.W., and Zucker, R.S. (1991). Presynaptic and serotonin-mediated enhancement of transmitter release at crayfish neuromuscular junction. J. Neurosci. *11*, 2631–2643.

del Castillo, J., and Katz, B. (1954). Quantal components of the endplate potential. J. Physiol. (Lond.) *124*, 560–573.

Dodge, F.A.J., and Rahamimoff, R. (1967). Co-operative action of calcium ions in transmitter release at the neuromuscular junction. J. Physiol. (Lond.) *193*, 419–432.

Dunlap, K., Luebke, J.I., and Turner, T.J. (1995). Exocytotic Ca^{2+} channels in mammalian central neurons. Trends Neurosci. *18*, 89–98.

Fields, R.D., Yu, C., and Nelson, P.G. (1991). Calcium, network activity, and the role of NMDA channels in synaptic plasticity. J. Neurosci. *11*, 134–146.

Frerking, M., Borges, S., and Wilson, M. (1995). Variation in GABA mini amplitude is the consequence of variation in transmitter concentration. Neuron *15*, 885–895.

Grynkiewicz, G., Poenie, M., and Tsien, R.Y. (1985). A new generation of Ca^{2+} indicators with greatly improved fluorescence properties. J. Biol. Chem. *260*, 3440–3450.

Hamill, O.P., Marty, A., Neher, E., Sakmann, B., and Sigworth, F. (1981). Improved patch-clamp techniques for high resolution current recordings from cells and cell-free membrane patches. Pflügers Arch. *391*, 85–100.

Harris, K.M. (1995). How multiple-synapse boutons could preserve input specificity during an interneuronal spread of LTP. Trends Neurosci. *18*, 365–369.

Heidelberger, R., Heinemann, C., Neher, E., and Matthews, G. (1994). Calcium dependence of the rate of exocytosis in a synaptic terminal. Nature *371*, 513–515.

Hessler, N.A., Shirke, A.M., and Malinow, R. (1993). The probability of transmitter release at a mammalian central synapse. Nature *366*, 569–572.

Hille, B. (1992). Ionic Channels of Excitable Membranes, Second Edition (Sunderland, Massachusetts: Sinauer Associates, Incorporated), pp. 321–326.

Jonas, P., Major, G., and Sakmann, B. (1993). Quantal components of unitary EPSPs at mossy fibre synapse on CA3 pyramidal cells of rat hippocampus. J. Physiol. (Lond.) *472*, 615–663.

Liao, D., Hessler, N.A., and Malinow, R. (1995). Activation of postsynaptically silent synapses during pairing-induced LTP in CA1 region of hippocampal slice. Nature *375*, 400–404.

Liu, G., and Tsien, R.W. (1995). Properties of synaptic transmission and single hippocampal synaptic boutons. Nature *375*, 404–408.

Lüscher, C., Streit, J., Lipp, P., and Lüscher, H.-R. (1994) Action potential conduction through embryonic dorsal root ganglion cells in culture. II. Decrease of conduction reliability during repetitive stimulation. J. Neurophysiol. *72*, 634–643.

Magee, J.C., and Johnston, D. (1995). Synaptic activation of voltage-gated channels in the dendrites of hippocampal pyramidal neurons. Science *268*, 301–304.

Malgaroli, A., Ting, A.E., Wendland, B., Bergamaschi, A., Villa, A., Tsien, R.W., and Scheller, R.H. (1995). Presynaptic component of long-term potentiation visualized at individual hippocampal synapses. Science *268*, 1624–1628.

Malinow, R. (1994). LTP: desperately seeking resolution. Science *266*, 1195–1196.

Malinow, R., and Tsien, R.W. (1990). Presynaptic enhancement shown by whole-cell recordings of long-term potentiation in hippocampal slices. Nature *346*, 177–180.

Malinow, R., Otmakhov, N., Blum, K.I., and Lisman, J. (1994). Visualizing hippocampal synaptic function by optical detection of Ca^{2+} entry through the N-methyl-D-aspartate channel. Proc. Natl. Acad. Sci. USA *91*, 8170–8174.

Minta, A., Kao, J., and Tsien, R.Y. (1989). Fluorescent indicators for cytosolic calcium based on rhodamine and fluorescein chromophores. J. Biol. Chem. *264*, 8171–8178.

Mintz, I.M., Sabatini, B.L., and Regehr, W.G. (1995). Calcium control of transmitter release at a cerebellar synapse. Neuron *15*, 675–688.

Murphy, T.H., and Baraban, J.M. (1990). Glutamate toxicity in immature cortical neurons precedes development of glutamate receptor currents. Dev. Brain Res. *57*, 146–150.

Murphy, T.H., Baraban, J.M., Wier, W.G., and Blatter, L.A. (1994). Visualization of quantal synaptic transmission by dendritic calcium imaging. Science *263*, 529–532.

Murphy, T.H., Baraban, J.M., and Wier, W.G. (1995). Mapping miniature synaptic currents to single synapses using calcium imaging reveals heterogeneity in postsynaptic output. Neuron *15*, 159–168.

Peters, A., Palay, S.L., and Webster, H.D. (1976). The Fine Structure of the Nervous System: The Neurons and Their Supporting Cells (Philadelphia: W.B. Saunders Company), pp. 90–117.

Pumplin, D.W., Reese, T.S., and Llinás, R. (1981). Are the presynaptic membrane particles the calcium channels? Proc. Natl. Acad. Sci. USA *78*, 7210–7213.

Raastad, M., Storm, J.F., and Andersen, P. (1992). Putative single quantum and single fibre excitatory postsynaptic currents show similar amplitude range and variability in rat hippocampal slices. Eur. J. Neurosci. *4*, 113–117.

Ragu, B., Murphy, E., Levy, L.A., Hall, R.D., and London, R.E. (1989). A fluorescent indicator for measuring cytosolic free magnesium. Am. J. Physiol. *256*, C540–C548.

Regehr, W.G., and Atluri, P.P. (1995). Calcium transients in cerebellar granule cell presynaptic terminals. Biophys. J. *68*, 2156–2170.

Regehr, W.G., Delaney, K.R., and Tank, D.W. (1994). The role of presynaptic calcium in short-term enhancement at the hippocampal mossy fiber synapse. J. Neurosci. *14*, 523–537.

Reuter, H. (1995). Measurements of exocytosis from single presynaptic nerve terminals reveal heterogeneous inhibition by Ca^{2+} channel blockers. Neuron *14*, 773–779.

Reynolds, E.S. (1963). The use of lead citrate at high pH as an electron opaque stain in electron microscopy. J. Cell Biol. *17*, 208–212.

Robitaille, R., Adler, E.M., and Charlton, M.P. (1990). Strategic location of calcium channels at transmitter release sites of frog neuromuscular synapses. Neuron *5*, 773–779.

Rosenmund, C., Clements, J.D., and Westbrook, G.L. (1993). Nonuniform probability of glutamate release at a hippocampal synapse. Science *262*, 754–757.

Ryan, T.A., and Smith, S.J. (1995). Vesicle pool mobilization during action potential firing at hippocampal synapses. Neuron *14*, 983–989.

Ryan, T.A., Reuter, H., Wendlan, B., Schweizer, F.E., Tsien, R.W.,

and Smith, S.J. (1993). The kinetics of synaptic vesicle recycling measured at single presynaptic boutons. Neuron *11*, 713–724.

Sheng, Z.-H., Rettig, J., Takahashi, M., and Catterall, W.A. (1994). Identification of a syntaxin-binding site on N-type calcium channels. Neuron *13*, 1303–1313.

Smith, S.J., and Augustine, G.J. (1988). Calcium ions, active zones and synaptic transmitter release. Trends Neurosci. *11*, 458–464.

Smith, S.J., Buchanan, J., Osses, L.R., Charlton, M.P., and Augustine, G.J. (1993). The spatial distribution of calcium signals in squid presynaptic terminals. J. Physiol. (Lond.) *472*, 573–593.

Sorra, K.E., and Harris, K.M. (1993). Occurrence and three-dimensional structure of multiple synapses between individual radium axons and their target pyramidal cells in hippocampal area CA1. J. Neurosci. *13*, 3736–3748.

Spruston, N., Schiller, Y., Stuart, G., and Sakmann, B. (1995). Activity-dependent action potential invasion and calcium influx into hippocampal CA1 dendrites. Science *268*, 297–300.

Stevens, C.F., and Wang, Y. (1994). Changes in reliability of synaptic function as a mechanism for plasticity. Nature *371*, 704–707.

Stevens, C.F., and Wang, Y. (1995). Facilitation and depression at single central synapses. Neuron *14*, 795–802.

Stuart, G.J., and Sakmann, B. (1994). Active propagation of somatic action potentials into neocortical pyramidal cell dendrites. Nature *367*, 69–72.

Takahashi, T., and Momiyama, A. (1993). Different types of calcium channels mediate central synaptic transmission. Nature *366*, 156–158.

Toth, P.T., Bindokas, V., Bleakman, D., Colmers, W.F., and Miller, R.J. (1993). Mechanism of presynaptic inhibition by neuropeptide Y at sympathetic nerve terminals. Nature *364*, 635–639.

Volgushev, M., Voronin, L.L., Chistiakova, M., Artola, A., and Singer, W. (1995). All-or-none excitatory postsynaptic potentials in the rat visual cortex. Eur. J. Neurosci. *7*, 1751–1760.

Wall, P.D. (1995). Do nerve impulses penetrate terminal arborizations? A pre-presynaptic control mechanism. Trends Neurosci. *18*, 99–103.

Wheeler, D.B., Randall, A., and Tsien, R.W. (1994). Roles of N-type and Q-type Ca^{2+} channels in supporting hippocampal synaptic transmission. Science *264*, 107–111.

Wu, L.-G., and Saggau, P. (1994a). Pharmacological identification of two types of presynaptic voltage-dependent calcium channels at CA3–CA1 synapses of the hippocampus. J. Neurosci. *14*, 5613–5622.

Wu, L.-G., and Saggau, P. (1994b). Adenosine inhibits evoked synaptic transmission primarily by reducing presynaptic calcium influx in area CA1 of hippocampus. Neuron *12*, 1139–1148.

Wu, L.-G., and Saggau, P. (1994c). Presynaptic calcium is increased during normal synaptic transmission and paired-pulse facilitation, but not in long-term potentiation in area CA1 of hippocampus. J. Neurosci. *14*, 645–654.

Yuste, R., and Denk, W. (1995). Dendritic spines as basic functional units of neuronal integration. Nature *375*, 682–684.

Zar, J.H. (1984). Biostatistical Analysis (Englewood Cliffs, New Jersey: Prentice Hall).

Zucker, R.S. (1993). Calcium and transmitter release. J. Physiol. (Paris) *87*, 25–36.